Research Square

Preprints are preliminary reports that have not undergone peer review.
They should not be considered conclusive, used to inform clinical practice,
or referenced by the media as validated information.

Dosiomics-based prediction of late genitourinary toxicity after Cyberknife for prostate cancer: a SHAP-explainable machine learning approach

Rocco Mottareale

rocco.mottareale@istitutotumori.na.it

Istituto Nazionale Tumori IRCCS "Fondazione G. Pascale"

Marcello Serra

Istituto Nazionale Tumori IRCCS "Fondazione G. Pascale"

Donato Pezzulla

Responsible Research Hospital

Savino Cilla

Gemelli Molise Hospital-Università Cattolica del Sacro Cuore

Valentina Borzillo

Istituto Nazionale Tumori IRCCS "Fondazione G. Pascale"

Esmeralda Scipilliti

Istituto Nazionale Tumori IRCCS "Fondazione G. Pascale"

Dario Franzese

Istituto Nazionale Tumori IRCCS "Fondazione G. Pascale"

Sisto Perdonà

Istituto Nazionale Tumori IRCCS "Fondazione G. Pascale"

Francesco Passaro

Istituto Nazionale Tumori IRCCS "Fondazione G. Pascale"

Alessandro Izzo

Istituto Nazionale Tumori IRCCS "Fondazione G. Pascale"

Sabrina Rossetti

Istituto Nazionale Tumori IRCCS "Fondazione G. Pascale"

Sandro Pignata

Istituto Nazionale Tumori IRCCS "Fondazione G. Pascale"

Gianluca Ametrano

Istituto Nazionale Tumori IRCCS "Fondazione G. Pascale"

Valentina d'Alesio

Istituto Nazionale Tumori IRCCS "Fondazione G. Pascale"

Francesca Buonanno

Istituto Nazionale Tumori IRCCS "Fondazione G. Pascale"

Cecilia Arrichiello
Istituto Nazionale Tumori IRCCS "Fondazione G. Pascale"

Simona Mercogliano
Istituto Nazionale Tumori IRCCS "Fondazione G. Pascale"

Rossella Di Franco
Istituto Nazionale Tumori IRCCS "Fondazione G. Pascale"

Vincenzo Ravo
Istituto Nazionale Tumori IRCCS "Fondazione G. Pascale"

Research Article

Keywords: Prostate cancer, Cyberknife SBRT, Machine Learning, Dosiomics, SHAP explainability

Posted Date: July 3rd, 2026

DOI: https://doi.org/10.21203/rs.3.rs-10090151/v1

License: This work is licensed under a Creative Commons Attribution 4.0 International License.
Read Full License

Additional Declarations: No competing interests reported.

Abstract

Objective

To evaluate whether organ-specific dosiomics extracted from CyberKnife® prostate SBRT plans can predict late genitourinary (GU) toxicity and to provide interpretable risk drivers using SHapley Additive exPlanations (SHAP) analysis.

Methods

Eighty-seven patients with localized prostate adenocarcinoma treated with CyberKnife® SBRT (35–36.25 Gy in five fractions) were retrospectively analyzed. Late GU toxicity was graded using the RTOG scale; the endpoint was grade ≥ 1 toxicity occurring ≥ 6 months after treatment (follow-up up to 5 years). DICOM RTDOSE/RTSTRUCT data were used to extract PyRadiomics dosiomics features from prostate, PTV, bladder, rectum, and penile bulb. After patient-level train/test splitting (80/20), feature filtering and LASSO selection were applied, a classifier was trained with group-aware cross-validation and class weighting. Model performance was assessed on an independent hold-out test set with bootstrap confidence intervals. SHAP analysis was used for explainability.

Results

Late GU toxicity occurred in 17.24% of patients. ROC-AUC was 0.85 ± 0.10 (95% CI 0.60–1.00) and accuracy was 0.88 ± 0.04 (95% CI 0.83–0.94). SHAP analysiss identified a compact set of plausible predictors reflecting both organ geometry and dose-pattern heterogeneity across prostate and bladder.

Conclusions

An explainable dosiomics-driven approach showed encouraging discrimination for late GU toxicity prediction after CyberKnife® prostate SBRT and provided clinically interpretable risk drivers. Multicenter validation is warranted to confirm generalizability.

Introduction

Prostate cancer (PCa) is among the most prevalent malignancies in the male population worldwide [1]. In this setting, radiotherapy plays a pivotal role and, over recent years, stereotactic body radiotherapy (SBRT) has progressively emerged as a key treatment option across multiple clinical scenarios of localized disease, enabled by the delivery of high doses per fraction over a limited number of sessions. From a radiobiological perspective, this approach is further supported by the low α/β ratio of PCa, which is lower than that of several adjacent normal tissues (e.g., bladder and rectum), suggesting a potential advantage of hypofractionation in terms of both efficacy and tolerability [2, 3]. The clinical adoption of

SBRT in PCa has been facilitated by major technological advances and, within this context, the CyberKnife (CK) platform has played a prominent role in many SBRT experiences for localized PCa [4–10]. The CK system, based on a robotic arm-mounted linear accelerator, enables real-time intrafraction prostate tracking through intraprostatic fiducial markers, adapting treatment delivery according to geometric information acquired during irradiation [8, 9]. In the literature, several studies on CK-based SBRT in predominantly low- and intermediate-risk patients, commonly using prescriptions of 35–36.25 Gy in five fractions, have reported favorable biochemical control rates and acute and late toxicity profiles broadly comparable to conventional external beam radiotherapy, albeit with variable follow-up [11–18]. Despite excellent oncological efficacy, treatment personalization remains a key priority, particularly with the aim of minimizing toxicity to organs at risk. In particular, late genitourinary (GU) toxicity, which may occur in the months following treatment, represents a clinically meaningful endpoint because it can substantially affect quality of life and is challenging to predict at the individual level. This underscores the need for predictive tools capable of early identification of patients at higher risk to develop late toxicity, thereby supporting planning choices and optimization strategies intended to reduce late adverse events without compromising disease control. Within this framework, radiomics and dosiomics have gained increasing attention as approaches capable of extracting complex quantitative information. Radiomics refers to the systematic extraction of quantitative features from medical images (e.g., CT or MRI), aiming to characterize patterns associated with tumor phenotype, treatment response, or toxicity risk. Dosiomics extends this paradigm to the dose distribution, treating the *dose map* as a source of quantitative descriptors that can capture heterogeneity, gradients, and spatial organization of dose. This rationale is particularly relevant in modern radiotherapy: plans with similar DVH metrics may still differ substantially in the spatial distribution of dose and its relationship to anatomy—differences that may be clinically consequential, especially for late toxicities. In prostate radiotherapy, models integrating radiomic, dosiomic, and clinical information have already been proposed to predict treatment response and support planning in IMRT contexts, for example distinguishing responders from non-responders [19], further highlighting the growing interest in multimodal and quantitative frameworks. Recent literature also indicates that dosiomics is emerging as a promising strategy to enhance predictive performance beyond traditional approaches, particularly in settings where the complexity of the dose distribution limits the utility of DVH-only indicators. In complex IMRT-treated sites such as head and neck, incorporating dosiomic features has been shown to improve prediction of clinical outcomes such as locoregional recurrence [20]. Similarly, dosiomics-based risk models have been proposed to predict radiation-induced adverse events and guide individualized treatment planning, such as temporal lobe injury [21]. In stereotactic settings, relevant contributions are also emerging: dosiomics models have been developed to predict treatment failures following lung SBRT by explicitly modelling interactions between dose characteristics and anatomical/imaging information [22], and approaches have investigated radiation pneumonitis prediction after SBRT using dosiomic features and/or deep learning–based radiomics extracted from 3D dose distributions [23, 24]. Interest in integrating radiomics, dosiomics, and DVH descriptors is also documented in other therapeutic contexts [25]. Despite these developments, targeted application of dosiomics in SBRT remains relatively underexplored and, importantly, evidence is still limited when focusing on clinically central scenarios such as CyberKnife-

based SBRT for PCa. This gap is particularly relevant: CK generates dose distributions with distinctive characteristics (steep dose gradients, high conformality, and a strong dependence on dose–anatomy interactions), which may plausibly influence late outcomes. Accordingly, the opportunity to extract and leverage these properties quantitatively through dosiomics may strengthen treatment personalization, especially when aimed at preventing late GU toxicity in the months following therapy. Beyond predictive performance, interpretability is a critical prerequisite for clinical adoption of machine learning models. In this context, explainable AI (XAI) is increasingly important: the goal is not only to predict an outcome, but also to clarify which variables drive the prediction and in what direction, thereby fostering trust, clinical validation, and potential use within a planning-oriented workflow. Among the most widely used explainability techniques, SHAP (SHapley Additive exPlanations) is becoming a reference standard for interpreting feature contributions both globally (average importance) and locally (patient-level explanations), and it is already employed in several radiotherapy and radiomics studies using interpretable modelling [26–29]. However, while explainability is increasingly integrated into radiomics workflows, evidence remains limited regarding systematic explainability of purely dosiomics-driven models. This is particularly relevant when the aim extends beyond risk stratification to identifying dosimetric patterns that may be modifiable at the planning stage.

The present study aims to contribute to a quantitative and clinically interpretable approach in the still underinvestigated context of CyberKnife-based SBRT for PCa. To our knowledge, this study is among the first to specifically investigate, in a cohort of PCa patients treated with CyberKnife SBRT, a dosiomics-driven predictive model for late genitourinary toxicity, with a SHAP-based explainability component to support clinical interpretability and transferability to treatment planning. The objective is to assess whether dosiomic features extracted from CyberKnife SBRT plans can predict late genitourinary toxicity (onset ≥ 6 months, grade ≥ 1) and to elucidate how dose-pattern and anatomy-related features contribute to the model's decisions. From this perspective, the study aims not only to explore the predictive capability of dosiomics, but also to promote its clinically oriented interpretability (Fig. 1).

Methods

Patient cohort, staging, and follow-up

Patients with localized prostate adenocarcinoma confirmed on biopsy were retrospectively identified. Diagnosis was established by transrectal core biopsy with at least 10 sampled cores, and all patients received CyberKnife® SBRT as definitive primary treatment. Eligibility was based on D'Amico risk classification: low-risk disease was defined as clinical stage ≤T2a with PSA ≤ 10 ng/mL and Gleason score ≤ 6, while intermediate-risk disease included stage T2b–T2c with PSA ≤ 20 ng/mL and Gleason score 7 (3 + 4). Patients with Gleason 7 (4 + 3) were not eligible. Only patients with a prostate volume ≤ 90 cc were included. Androgen deprivation therapy (ADT) was not part of the institutional treatment protocol; nevertheless, some patients received a short course of ADT (up to 3 months) at the discretion of the treating urologist, and ADT was not administered during or after radiotherapy. Staging

investigations comprised multiparametric prostate MRI when possible (pelvic CT in cases of contraindication), along with CT imaging of the abdomen and chest and a bone scan.

A total of 87 patients were included. Late GU toxicity was assessed using the Radiation Therapy Oncology Group (RTOG) toxicity scale [30]. Patients were followed for up to five years and were classified as positive if they developed late GU toxicity grade ≥ 1 occurring ≥ 6 months after treatment. Overall, 17.24% of patients developed late GU toxicity fulfilling the endpoint definition, whereas biochemical recurrence occurred in only 4.59%, consistent with the high level of disease control achieved with CyberKnife SBRT.

Fiducial implantation and simulation

Four gold fiducial markers were placed transperineally within the prostate under transrectal ultrasound guidance, arranged in an approximately triangular configuration. During each treatment fraction, the fiducials were continuously monitored to capture both translational and rotational motion, and the system automatically adjusted beam targeting whenever displacement was detected. After a 7–10 days interval to allow marker stabilization, patients underwent non-contrast CT simulation for treatment planning (1-mm slice thickness) in the supine position using individualized immobilization (Vac-Lok).

Target and OAR delineation

Target volumes were contoured on the planning CT with co-registered MRI. For low-risk cases, the GTV comprised the prostate alone, whereas for intermediate-risk disease it included the prostate together with the proximal 2 cm of the seminal vesicles. The CTV was set equal to the GTV. A PTV margin was then applied by expanding the CTV by 3 mm posteriorly and 5 mm in all remaining directions. Organs at risk were delineated, including the rectum, bladder, penile bulb, femoral heads, bowel, testes, and the neurovascular bundle.

SBRT treatment planning and prescription

Treatment plans were generated with the Accuray Precision® inverse planning platform (Accuray Inc., Sunnyvale, CA, USA). A total dose of 35–36.25 Gy was prescribed and delivered in five fractions (7–7.25 Gy per fraction), normalized to the 80% isodose line, with the aim of encompassing at least 95% of the PTV. Dose–volume constraints for organs at risk are summarized in Table 1. Late GU toxicity rates did not significantly differ between prescription dose groups (35 vs 36.25 Gy), with incidences of 19.51% and 22.58%, respectively (χ^2 test, $p = 0.798$).

Table 1
Dose–volume constraints for organs at risk (OARs) used in CyberKnife® prostate SBRT planning. Constraints are reported as maximum dose (Dmax) and/or volume-based limits (VxGy or Vx%) as specified.

OAR	Dmax	Dose limit
Bladder		V37Gy < 10 ccV37.5Gy < 5 ccV50% < 40%V100% < 10%
Rectum	< 38 Gy	V36Gy < 1 ccV25Gy < 20 ccV50% < 50%V80% < 20%V90% < 10%V100% < 5%
Penile bulb		V29Gy < 50%V30Gy < 3 cc
Femoral head		V14.5Gy < 5% (bilateral)
Testes		D20% < 2 Gy
Neurovascular bundle		V49Gy < 10%
Bowel		V29.5Gy < 10%V30Gy < 1 cc

Treatment delivery and image guidance

Treatment was delivered every other day using the CyberKnife® platform, which integrates a 6-MV linear accelerator mounted on a six-degrees-of-freedom robotic system. This configuration permits non-coplanar irradiation from a large set of predefined beam nodes yielding a highly heterogeneous set of beam entry angles. Pronounced intratarget dose heterogeneity (with peak doses exceeding the prescription within the target) and steep dose gradients are intrinsic features of CyberKnife delivery. Image guidance was performed with a stereoscopic X-ray system comprising two orthogonally oriented, ceiling-mounted X-ray sources coupled to floor-mounted flat-panel detectors. Imaging was repeated at approximately 45–60s intervals; acquired images were registered to digitally reconstructed radiographs derived from the planning CT to identify intra-fraction motion and to trigger automatic, real-time corrections during irradiation.

Dosiomic features extraction

For each patient, planning CT images, structure sets (RTSTRUCT), and physical dose distributions (RTDOSE) were retrieved in DICOM format. CT images were acquired using a helical protocol with 1.0-mm slice thickness and an in-plane pixel spacing of 1.367 × 1.367 mm², providing high spatial resolution suitable for SBRT planning and dose–anatomy analysis. All datasets shared a common frame of reference, ensuring spatial consistency among anatomy, delineated structures, and dose. The three-dimensional physical dose distribution (in Gy) was exported from the treatment planning system and converted into a 3D grayscale image volume. Absolute dose values were preserved by applying the DICOM Dose Grid Scaling factor, and the original dose grid resolution and voxel geometry were retained; no resampling or interpolation was performed to avoid smoothing the steep dose gradients

characteristic of SBRT. Dosiomic feature extraction was performed using PyRadiomics, treating the dose distribution as a quantitative imaging modality and using RTSTRUCT-derived masks to define regions of interest (ROIs). Five clinically relevant ROIs were analyzed—Prostate, Planning Target Volume (PTV), Rectum, Bladder, and Penile bulb—selected based on their anatomical proximity and plausible mechanistic relevance to GU toxicity. For each ROI, 76 features were extracted and grouped as follows: (i) shape and geometric descriptors computed from the ROI mask only (n = 18); (ii) first-order statistics computed from voxel-wise dose values within the ROI (n = 18); (iii) texture features derived from the Gray Level Co-occurrence Matrix (GLCM) computed on the dose values within the ROI (n = 24); and (iv) texture features derived from the Gray Level Run Length Matrix (GLRLM) computed on the dose values within the ROI (n = 16). All features were aggregated into a wide, patient-level feature matrix by concatenating feature names with ROI identifiers to preserve organ-specific interpretability.

Data preparation

The dataset comprised dosiomic features extracted per organ and a binary outcome label for late GU toxicity. Data were split at the patient level into training (80%) and independent hold-out test (20%) sets. Missing values were imputed with the median estimated on the training set and applied unchanged to the test set. Dimensionality reduction was performed using a multistep filtering strategy applied strictly within the training data. Highly collinear features were removed based on pairwise Pearson correlation ($|\rho| > 0.95$), and quasi-constant features were excluded using a coefficient of variation (CV) threshold of 0.05. Remaining features were standardized using z-score normalization using training-set parameters applied to both sets.

Model Development

Extreme Gradient Boosting (XGBoost) was employed as the machine learning algorithm for the prediction of late GU toxicity. XGBoost is an ensemble learning method based on gradient-boosted decision trees, in which a strong predictive model is constructed by iteratively combining multiple weak learners. At each boosting iteration, a new tree is trained to model the residual errors of the current ensemble, thereby progressively improving discrimination performance. For a patient *i*, with feature vector $x_i \in R^P$ (i.e., the dimensionality of the feature space), the model first computes a raw score (logit), $\mathrm{z}_i = \sum_{k=1}^{K} f_k(x_i)$, where each f_k denotes a regression tree. The predicted probability of late GU toxicity is then obtained by logistic function, $\hat{y}_i = \sigma(\mathrm{z}_i) = 1/(1+e^{-\mathrm{z}_i})$. The set of trees $\{f_k\}$ is learned by minimizing a regularized objective function $\mathcal{L} = \sum_{i=1}^{n} l(y_i, \hat{y}_i) + \sum_{k=1}^{K} \Omega(f_k)$, where $y_i \in \{0,1\}$ is the observed outcome (absence/presence of late GU toxicity), $l(\cdot)$ is the logistic loss, and $\Omega(\cdot)$ penalizes tree complexity. This regularization framework mitigates overfitting and enables robust learning in high-dimensional settings. Owing to its ability to capture nonlinear effects and high-order interactions among predictors, XGBoost is particularly well suited for dosiomic data, where complex spatial patterns of dose distribution are expected to influence toxicity outcomes. Following

correlation-based and variability-based feature filtering, L1-regularized logistic regression (LASSO) was applied for sparse feature selection, yielding a compact subset of 20 predictors as input to the XGBoost model. Hyperparameter optimization was conducted exclusively on the training cohort using GridSearchCV (scikit-learn), with model performance quantified by ROC-AUC. Cross-validation was implemented using a 5-fold GroupKFold strategy, with Patient_ID specified as the grouping variable, ensuring that all observations from the same patient were confined to a single fold during tuning. This design preserved patient-level independence across folds and prevented optimistic bias in performance estimation. After selection of the optimal hyperparameter configuration, the XGBoost model was refit on the entire training set. Class imbalance was addressed by incorporating the scale_pos_weight parameter, computed as the ratio of negative to positive cases in the training set. This approach was preferred over synthetic oversampling because it preserves the original data distribution. The finalized model was evaluated on the independent hold-out test set. Discriminative performance was primarily assessed using ROC-AUC, complemented by standard classification metrics including accuracy, precision, recall, and F1-score. A stratified bootstrap procedure with repeated patient-level resampling provided confidence intervals for ROC-AUC and accuracy.

Model Explainability

To enhance transparency and clinical interpretability of the XGBoost predictions, SHAP analysis was employed to provide both global and local explanations of model behaviour. SHAP is a model-agnostic explainability framework grounded in cooperative game theory, in which each input feature is interpreted as a player contributing to the final prediction. Formally, for each patient *i*, SHAP assigns to each feature j a numerical value ϕ_{ij} quantifying its average marginal contribution to the model output, computed across all possible feature coalitions. Mathematically, the Shapley value is defined as $\phi_{ij} = \sum_{S \subseteq F \setminus \{j\}} \{|S|!(p-|S|-1)!/p!\} \bullet [f_{S\cup\{j\}}(xi) - f_S(xi)]$, where $F = \{1, \ldots, p\}$ is the full feature set, S⊆F\{j} a subset of features excluding j and $f_S(x_i)$ denotes the model output when conditioned on features in S. SHAP values were estimated using *KernelExplainer*, a model-agnostic estimator suitable for probabilistic classifiers. The explainer was initialized on a representative background of $m = 50$ patients randomly sampled from the training set, defining the baseline model output $\phi_0 = 1/m \sum_{k=1}^{m} \hat{y}\left(x^{(k)}\right)$, where $x^{(k)} \in R^P$ denotes the feature vector of the *k*-th background patient and $\hat{y}\left(x^{(k)}\right)$ is the corresponding model-predicted probability. For each patient *i*, SHAP provides a local additive decomposition of the predicted probability, $\hat{y}_i = \phi_0 + \sum_{j=1}^{p} \phi_{ij}$, where ϕ_{ij} represents the feature-specific contribution, positive or negative, to the patient-specific risk estimate. Shapley values were approximated via Monte Carlo sampling of up to 200 feature coalitions per patient, applied to both training and test sets. Explanations were generated directly on the predicted probability of late GU toxicity, enabling clinically meaningful interpretation. Global model interpretability was assessed by ranking features according to their mean absolute SHAP value, $I_j = 1/n \sum_{i=1}^{n} \left|\phi_{ij}\right|$, and visualized using beeswarm and bar plots, highlighting both feature importance and the directionality of their effects. Local interpretability was evaluated at the individual patient level by

decomposing each predicted probability into the baseline risk plus the sum of feature-specific SHAP contributions. Patient-level force plots were generated to identify the dominant drivers of each prediction.

Results

3.1 Features selection

After pivoting, the final dataset consisted of 87 patients described by 380 dosiomic features (76 per anatomical structure · 5 structures). Correlation-based filtering removed 172 highly correlated features, leaving 208 features (Fig. 2). Subsequent low variability-based filtering excluded 70 quasi-constant features, yielding 138 features entering the selection stage. LASSO-based sparse selection on the training data produced a final subset of 20 predictors. Overall, the sequential strategy reduced the original feature space by ∼95%, retaining descriptors spanning shape, first-order dose statistics, and texture features across multiple structures.

3.2 ML model performance

The optimized XGBoost model demonstrated good discrimination in predicting late GU toxicity on the independent hold-out test set. Patient-level stratified bootstrap resampling was applied to quantify uncertainity. The mean ROC-AUC across bootstrap resamples was 0.85 ± 0.10 (95% CI: 0.60–1.00), while mean accuracy was 0.88 ± 0.04 (95% CI: 0.83–0.94). The corresponding ROC curve with bootstrap-derived variability is shown in Fig. 3. Class-wise evaluation showed high specificity for patients without late toxicity, with perfect recall for the negative class, whereas sensitivity for the minority toxicity class was lower (recall = 0.33). Precision for the positive class was high (1.00), resulting in an F1-score of 0.50, consistent with the challenge of detecting rare late toxicity events in a small, imbalance-corrected cohort.

3.3 SHAP analysis

The beeswarm plot in Fig. 4 ranks features by mean absolute SHAP value; each point represents one patient–feature pair, with color encoding feature magnitude. For the top-ranked features, SHAP values stratified coherently along the color gradient, indicating a stable and biologically interpretable relationship between feature intensity and predicted risk. The SHAP decision plot on the training set (Fig. 5) shows cumulative feature contributions as polylines per patient; trajectories diverged progressively from the baseline expected value, with a clear separation between low- and high-output paths emerging within the first 4–5 features, whereas the remaining features contributed only minor incremental refinements. Local interpretability was assessed through single-patient SHAP decision plots (Fig. 6), with patient-specific feature values annotated at each step. In the representative true negative (TN) case, the cumulative path progressed from the baseline value (~ 0.2) to a low predicted probability (~ 0.05); in the true positive (TP) case, the path moved to a high predicted probability (~ 0.80). In both examples, the largest stepwise shifts occurred within the first 4–5 features, accounting for approximately 70–80% of the total change.

Discussion

In this study, we developed a machine learning framework integrating dosiomic feature engineering, gradient-boosted tree modelling, and SHAP-based explainability to predict late GU toxicity following prostate SBRT. The clinical motivation arises from the high disease control typically achieved with CyberKnife SBRT juxtaposed with the persistent risk of late GU toxicity that can adversely affect long-term quality of life. Accordingly, our objective was not only to build a proof-of-concept predictive model using complex dosiomic descriptors, but also to provide an interpretable representation of how dose- and anatomy-related patterns contribute to individual risk, supporting potential translation toward risk-adapted planning. In this setting, the XGBoost model demonstrated encouraging discriminatory ability on the independent hold-out cohort, with performance stability supported by bootstrap resampling. Class-specific metrics indicated excellent identification of the of the non-toxicity majority class. Conversely, sensitivity for the minority late-toxicity class remained lower despite class weighting. Precision for the positive class was high, suggesting that positive predictions are typically reliable. Overall, the model appears conservative in calling toxicity, an expected limitation when modelling rare late outcomes in small cohorts. Interpretability analyses provided mechanistic insight into model behavior. Consequently, first-order and texture features quantify the statistical distribution and spatial organization of dose within each ROI, whereas shape features depend exclusively on mask geometry and act as anatomical proxies that can indirectly modulate dose exposure and planning complexity.

Within this framework, SHAP highlighted a compact set of dominant, physically plausible drivers. The bladder maximum 2D diameter (row direction) emerged as the most influential variable; higher values increased predicted toxicity risk. As an anatomical shape descriptor, this finding suggests that specific bladder geometries (greater planar extent/distension) constitute scenarios in which dose spill or steep gradients are more likely to involve clinically relevant bladder subregions, particularly the base/neck. Consistently, the bladder GLRLM normalized run-length non-uniformity was associated with increased risk at higher values, indicating that not only dose amount but also its spatial patterning within the bladder matters: elevated run-length non-uniformity reflects a more fragmented intravesical dose pattern, compatible with localized hotspots and complex gradients. From a biological standpoint, such fragmentation is more compatible with localized high-dose subregions than with coldspots, making heterogeneous intravesical dose patterning a plausible contributor to late radiation injury.

On the target side, lower prostate first-order IQR was associated with higher risk; as this descriptor captures intraprostatic dose dispersion, the directionality is consistent with the hypothesis that reduced intraprostatic dose variability may reflect less SBRT-like configurations potentially limiting gradient control and increasing dose involvement of GU-sensitive regions.

Anatomical proxies of geometric complexity were coherently linked to risk: higher prostate flatness appeared protective, suggesting that regular prostate morphology facilitates conformal isodose shaping, whereas higher rectum major axis length was associated with increased risk, consistent with rectal

elongation/distension altering spatial relationships and gradient management in highly conformal plans. Agreement between global and local explanations further supports internal consistency.

Overall, these findings suggest that the model captures anatomical factors (shape) modulating critical subregion exposure and dose-pattern factors (first-order/texture) quantifying dose irregularity within relevant ROIs. SHAP reflects model-learned associations rather than causality, and complementary analyses on alternative plans are warranted to verify whether reducing localized dose irregularity/hotspots in specific ROIs yields robust decreases in predicted risk while maintaining oncologic target coverage.

This study has several limitations. Residual overfitting cannot be excluded given the small cohort size and low prevalence of late toxicity events. The single-institution design means that variations in imaging protocols, structure delineation, dose calculation and outcome assessment across centers may affect feature distributions and model transportability. The reduced recall for the minority toxicity class further underscores the need for larger cohorts and external validation. Future work will focus on multicenter validation, integration of clinical covariates, and assessment of longitudinal toxicity trajectories. Despite these limitations, the proposed framework demonstrates the feasibility of combining dosiomics-driven prediction with rigorous explainability, providing both cohort-level insights and patient-specific decompositions that can support transparent risk stratification and, ultimately, personalized radiotherapy planning.

Conclusions

An explainable dosiomics-based machine learning pipeline was implemented to predict late GU toxicity after prostate SBRT, integrating rigorous patient-level preprocessing, XGBoost modelling, and SHAP-driven interpretation. To the best of our knowledge, this study represents one of the first evaluations of dosiomics combined with SHAP-based explainability for late GU toxicity prediction in the specific context of CyberKnife prostate SBRT. The model showed encouraging discrimination on an independent hold-out cohort; SHAP analysis identified a compact set of physically plausible anatomical and dose-pattern descriptors, supporting the potential utility of the framework for transparent risk stratification and planning support. Given the limited cohort size and low prevalence of late toxicity events, multicenter validation on larger datasets is warranted to confirm generalizability.

Declarations

Competing interests

The authors declare that the research was conducted in the absence of any commercial or financial relationships that could be construed as a potential conflict of interest.

Ethics approval and consent to participate

This study was conducted within the framework of the CyPro Trial (CyberKnife Prostate cancer), protocol number 46/19, which was formally approved by the Ethics Committee of the Istituto Nazionale Tumori IRCCS Fondazione G. Pascale (Naples, Italy) on January 15, 2020 (Decree n. 105 of February 12, 2020). The study was performed in accordance with the Declaration of Helsinki, local legislation, and institutional requirements. In accordance with national legislation and institutional guidelines, the requirement for written informed consent for participation was waived by the Ethics Committee. Written informed consent was obtained from the individuals for the publication of any potentially identifiable images or data included in this article.

Consent for publication

Written informed consent was obtained from the individuals concerned for the publication of any potentially identifiable images or clinical data included in this article.

Funding

The authors declare financial support was received for the research, authorship, and/or publication of this article. This work was supported by the Italian Ministry of Health Ricerca Corrente funds. Research Project LINEA 4/15_25, Istituto Nazionale Tumori-IRCCS-Fondazione G. Pascale.

Author Contribution

Conceptualization: RM, MS, RDF; Methodology: RM, MS, RDF, DP, SC; Formal analysis and data curation: RM, MS, SC; Investigation and clinical data collection: RDF, VB, ES; Writing - original draft preparation: RM, MS, RDF; Writing - review and editing: RM, MS, DP, SC, VB, ES, DF, SP, FP, AI, SR, SPi, GA, VD, FB, CA, SM, RDF, VR; Supervision: RDF, VR. All authors have read and agreed to the published version of the manuscript.

Acknowledgement

The authors thank Alessandra Trocino, librarian at the Istituto Nazionale Tumori di Napoli, IRCCS “G. Pascale”, Italy, for bibliographic assistance

Data Availability

Original datasets are available in a publicly accessible repository: Zotero. The original contributions presented in the study are publicly available. The data will be available as raw data to URL: Stereotactic Body Radiotherapy with Cyberknife® System for Low-and Intermediate-Risk Prostate Cancer. Clinical

Outcomes and Toxicities of CyPro Trial — Zenodo (DOI 10.5281/zenodo.8187900, accessed on 26 Jul 2023).

References

1. Ferlay J, Ervik M, Lam F, Laversanne M, Colombet M, Mery L, Piñeros M, Znaor A, Soerjomataram I, Bray F. (2024). Global Cancer Observatory: Cancer Today (version 1.1). Lyon, France: International Agency for Research on Cancer. Available from: https://gco.iarc.who.int/today, accessed [December 2025].
2. Miralbell R, Roberts SA, Zubizarreta E, Hendry JH. Dose-Fractionation Sensitivity of Prostate Cancer Deduced From Radiotherapy Outcomes of 5,969 Patients in Seven International Institutional Datasets: α/β = 1.4 (0.9–2.2) Gy. Int J Radiation Oncology*Biology*Physics. 2012;82:e17–24. https://doi.org/10.1016/j.ijrobp.2010.10.075.
3. Dasu A, Toma-Dasu I. Prostate alpha/beta revisited – an analysis of clinical results from 14 168 patients. Acta Oncol. 2012;51:963–74. https://doi.org/10.3109/0284186X.2012.719635.
4. King CR, Lehmann J, Adler JR, Hai J. CyberKnife Radiotherapy for Localized Prostate Cancer: Rationale and Technical Feasibility. Technol Cancer Res Treat. 2003;2:25–9. https://doi.org/10.1177/153303460300200104.
5. Katz AJ. CyberKnife Radiosurgery for Prostate Cancer. Technol Cancer Res Treat. 2010;9:463–72. https://doi.org/10.1177/153303461000900504.
6. Miszczyk L, Namysł-Kaletka A, Napieralska A et al. (2017) Cyberknife Radioablation of Prostate Cancer – Preliminary Results for 400 Patients. APJCP 18:. https://doi.org/10.22034/APJCP.2017.18.4.1007
7. Serra M, De Martino F, Savino F, et al. SBRT for Localized Prostate Cancer: CyberKnife vs. VMAT-FFF, a Dosimetric Study. Life. 2022;12:711. https://doi.org/10.3390/life12050711.
8. Borzillo V, Scipilliti E, Pezzulla D, et al. Stereotactic body radiotherapy with CyberKnife® System for low- and intermediate-risk prostate cancer: clinical outcomes and toxicities of CyPro Trial. Front Oncol. 2023;13:1270498. https://doi.org/10.3389/fonc.2023.1270498.
9. Gagliardo G, Serra M, Ametrano G, et al. Evaluating dosimetric outcomes: a comparison of CyberKnife, VMAT FFF, and Helical Tomotherapy Radixact for treating localized prostate cancer. Radiol med. 2025. https://doi.org/10.1007/s11547-025-02046-3.
10. (2025) Lower incidence of sexual dysfunction associated with stereotactic radiosurgery using CyberKnife in prostate cancer patients: initial resultsMenor incidencia de disfunción sexual asociada a la radiocirugía estereotáctica con CyberKnife en pacientes con cáncer de próstata: resultados iniciales. RIA 23:79. https://doi.org/10.22514/j.androl.2025.033
11. Katz AJ, Santoro M, Diblasio F, Ashley R. Stereotactic body radiotherapy for localized prostate cancer: disease control and quality of life at 6 years. Radiat Oncol. 2013;8:118. https://doi.org/10.1186/1748-717X-8-118.

12. Chen LN, Suy S, Uhm S, et al. Stereotactic Body Radiation Therapy (SBRT) for clinically localized prostate cancer: the Georgetown University experience. Radiat Oncol. 2013;8:58. https://doi.org/10.1186/1748-717X-8-58.
13. Katz AJ, Kang J. Stereotactic Body Radiotherapy as Treatment for Organ Confined Low- and Intermediate-Risk Prostate Carcinoma, a 7-Year Study. Front Oncol. 2014;4. https://doi.org/10.3389/fonc.2014.00240.
14. King CR, Freeman D, Kaplan I, et al. Stereotactic body radiotherapy for localized prostate cancer: Pooled analysis from a multi-institutional consortium of prospective phase II trials. Radiother Oncol. 2013;109:217–21. https://doi.org/10.1016/j.radonc.2013.08.030.
15. Katz A. (2017) Stereotactic Body Radiotherapy for Low-Risk Prostate Cancer: A Ten-Year Analysis. Cureus. https://doi.org/10.7759/cureus.1668
16. Bolzicco G, Favretto MS, Satariano N, et al. A single-center study of 100 consecutive patients with localized prostate cancer treated with stereotactic body radiotherapy. BMC Urol. 2013;13:49. https://doi.org/10.1186/1471-2490-13-49.
17. Abramowitz MC, Li T, Buyyounouski MK, et al. The Phoenix definition of biochemical failure predicts for overall survival in patients with prostate cancer. Cancer. 2008;112:55–60. https://doi.org/10.1002/cncr.23139.
18. Katz A, Formenti SC, Kang J. Predicting Biochemical Disease-Free Survival after Prostate Stereotactic Body Radiotherapy: Risk-Stratification and Patterns of Failure. Front Oncol. 2016;6. https://doi.org/10.3389/fonc.2016.00168.
19. Yu Y, Chen D, Zhu Y. Multi-modal predictive modeling in prostate cancer radiotherapy: A radiomics and dosiomics approach. J Radiation Res Appl Sci. 2025;18:101518. https://doi.org/10.1016/j.jrras.2025.101518.
20. Wu A, Li Y, Qi M, et al. Dosiomics improves prediction of locoregional recurrence for intensity modulated radiotherapy treated head and neck cancer cases. Oral Oncol. 2020;104:104625. https://doi.org/10.1016/j.oraloncology.2020.104625.
21. Yang S-S, OuYang P-Y, Guo J-G, et al. Dosiomics Risk Model for Predicting Radiation Induced Temporal Lobe Injury and Guiding Individual Intensity-Modulated Radiation Therapy. Int J Radiation Oncology*Biology*Physics. 2023;115:1291–300. https://doi.org/10.1016/j.ijrobp.2022.11.036.
22. Bhandari A, Johnson K, Oh K, et al. Developing a novel dosiomics model to predict treatment failures following lung stereotactic body radiation therapy. Front Oncol. 2024;14:1438861. https://doi.org/10.3389/fonc.2024.1438861.
23. Huang Y, Feng A, Lin Y, et al. Radiation pneumonitis prediction after stereotactic body radiation therapy based on 3D dose distribution: dosiomics and/or deep learning-based radiomics features. Radiat Oncol. 2022;17:188. https://doi.org/10.1186/s13014-022-02154-8.
24. Zhang Z, Wang Z, Yan M, et al. Radiomics and Dosiomics Signature From Whole Lung Predicts Radiation Pneumonitis: A Model Development Study With Prospective External Validation and

Decision-curve Analysis. Int J Radiation Oncology*Biology*Physics. 2023;115:746–58. https://doi.org/10.1016/j.ijrobp.2022.08.047.

25. Mansouri Z, Salimi Y, Hajianfar G, et al. Potential of Radiomics, Dosiomics, and Dose Volume Histograms for Tumor Response Prediction in Hepatocellular Carcinoma following 90Y-SIRT. Mol Imaging Biol. 2025;27:201–14. https://doi.org/10.1007/s11307-025-01992-8.
26. Cilla S, Rossi R, Habberstad R, et al. Explainable Machine Learning Model to Predict Overall Survival in Patients Treated With Palliative Radiotherapy for Bone Metastases. JCO Clin Cancer Inf e2400027. 2024. https://doi.org/10.1200/CCI.24.00027.
27. Cilla S, Romano C, Macchia G, et al. Radiomics-based explainable artificial intelligence to predict treatment response following lung stereotactic body radiation therapy. Br J Radiol. 2025;98:1988–96. https://doi.org/10.1093/bjr/tqaf043.
28. Aymerich M, García-Baizán A, Franco PN, et al. Radiomics-Based Classification of Clear Cell Renal Cell Carcinoma ISUP Grade: A Machine Learning Approach with SHAP-Enhanced Explainability. Diagnostics. 2025;15:1337. https://doi.org/10.3390/diagnostics15111337.
29. Wang Y, Liu X, Zhao X, et al. A radiomics-based machine learning model and SHAP for predicting spread through air spaces and its prognostic implications in stage I lung adenocarcinoma: a multicenter cohort study. Cancer Imaging. 2025;25:115. https://doi.org/10.1186/s40644-025-00935-4.
30. Meier RM, Bloch DA, Cotrutz C, et al. Multicenter Trial of Stereotactic Body Radiation Therapy for Low- and Intermediate-Risk Prostate Cancer: Survival and Toxicity Endpoints. Int J Radiation Oncology*Biology*Physics. 2018;102:296–303. https://doi.org/10.1016/j.ijrobp.2018.05.040.

Figures

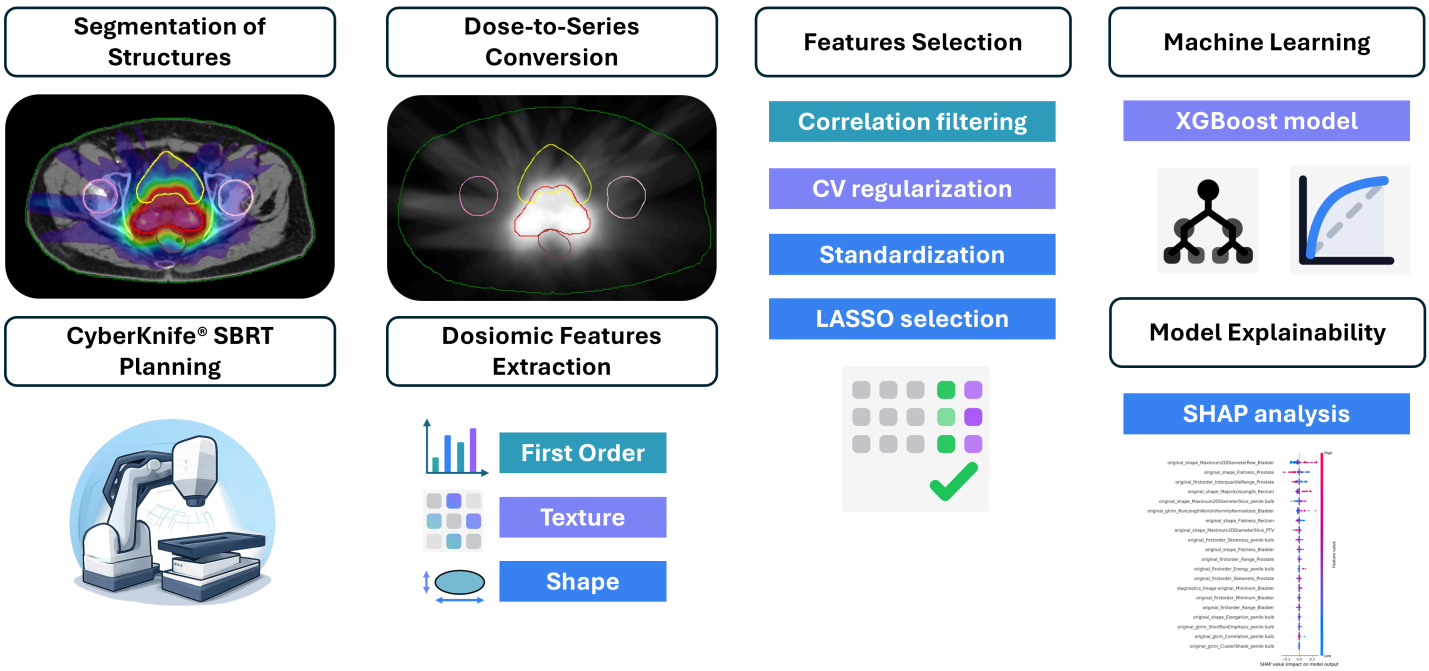


Figure 1

Flowchart of the study methodological workflow: anatomical structures (bladder, penile bulb, rectum, prostate, and PTV) were segmented and CyberKnife SBRT planning was performed to obtain dose distributions. Dose data were converted into 3D series for dosiomic feature extraction (first-order, texture, and shape classes). Feature selection included correlation filtering ($|\rho| > 0.95$), coefficient of variation thresholding (CV < 0.05), standardization, and LASSO regression. The selected features were used to train an XGBoost machine learning model, while SHAP analysis was applied for model explainability and feature relevance assessment. Abbreviations: SBRT = Stereotactic Body Radiation Therapy; CV = Coefficient of Variation; LASSO = Least Absolute Shrinkage and Selection Operator; XGBoost = eXtreme Gradient Boosting; SHAP = SHapley Additive exPlanations.



Figure 2

Feature correlation matrix before (left) and after (right) filtering. Heatmap of Pearson correlation coefficients among the 380 initial dosiomic features (76 for each of the five considered anatomical structures: Prostate, PTV, Rectum, Bladder, and Penile bulb). Colors indicate correlation intensity, with red for positive ($\rho \rightarrow +1$), blue for negative ($\rho \rightarrow -1$), and white for weak/no correlation ($\rho \approx 0$). Before filtering, dense red–blue blocks reveal strong multicollinearity within and across feature groups. After filtering ($|\rho| > 0.95$), the correlation structure becomes visibly sparser, confirming effective redundancy reduction prior to feature selection.

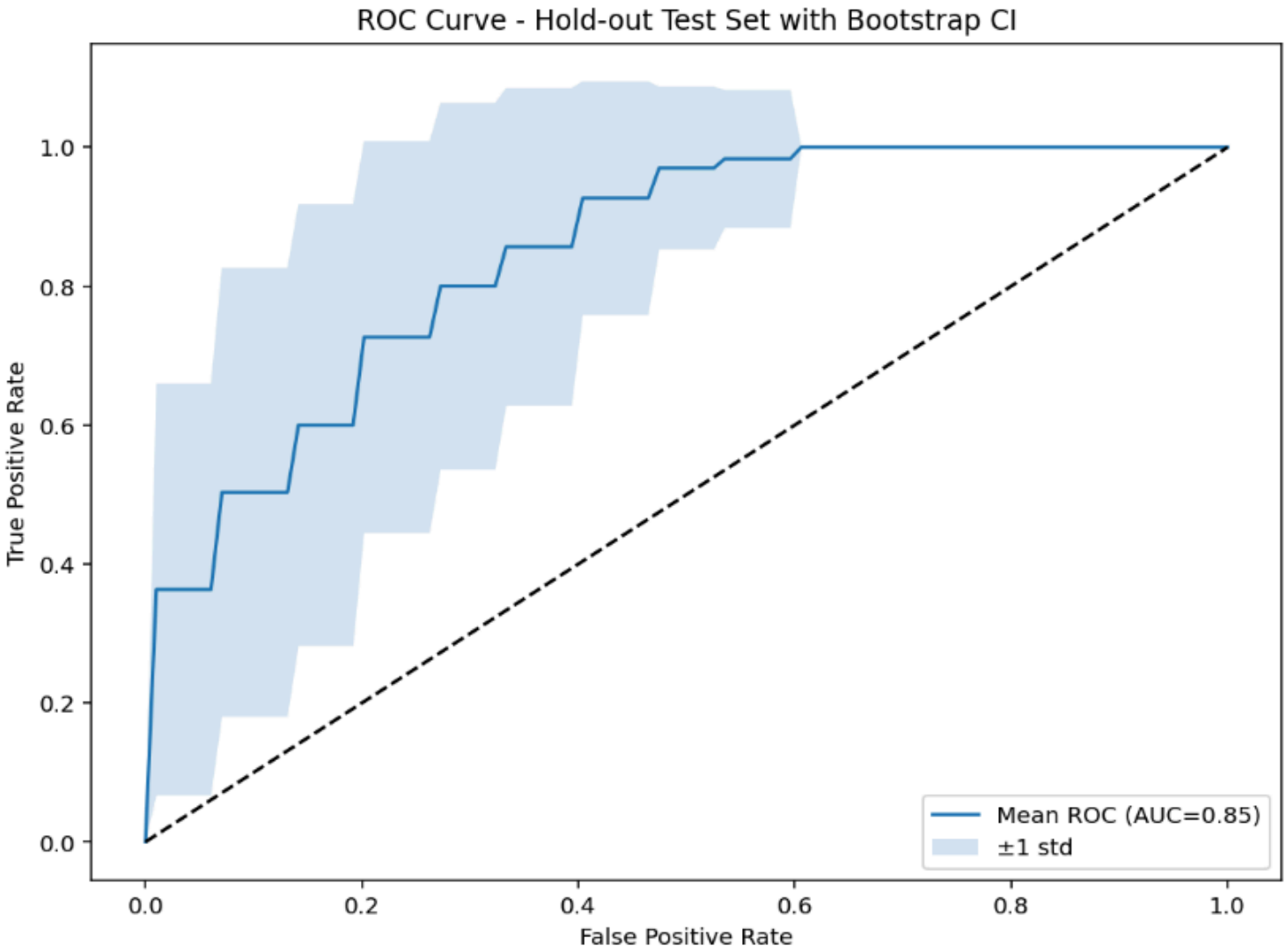


Figure 3

Receiver operating characteristic (ROC) curve of the optimized XGBoost model evaluated on the independent hold-out test set. The solid line represents the mean ROC curve across bootstrap resamples, while the shaded area denotes ±1 standard deviation (std). The dashed diagonal line indicates chance-level performance.

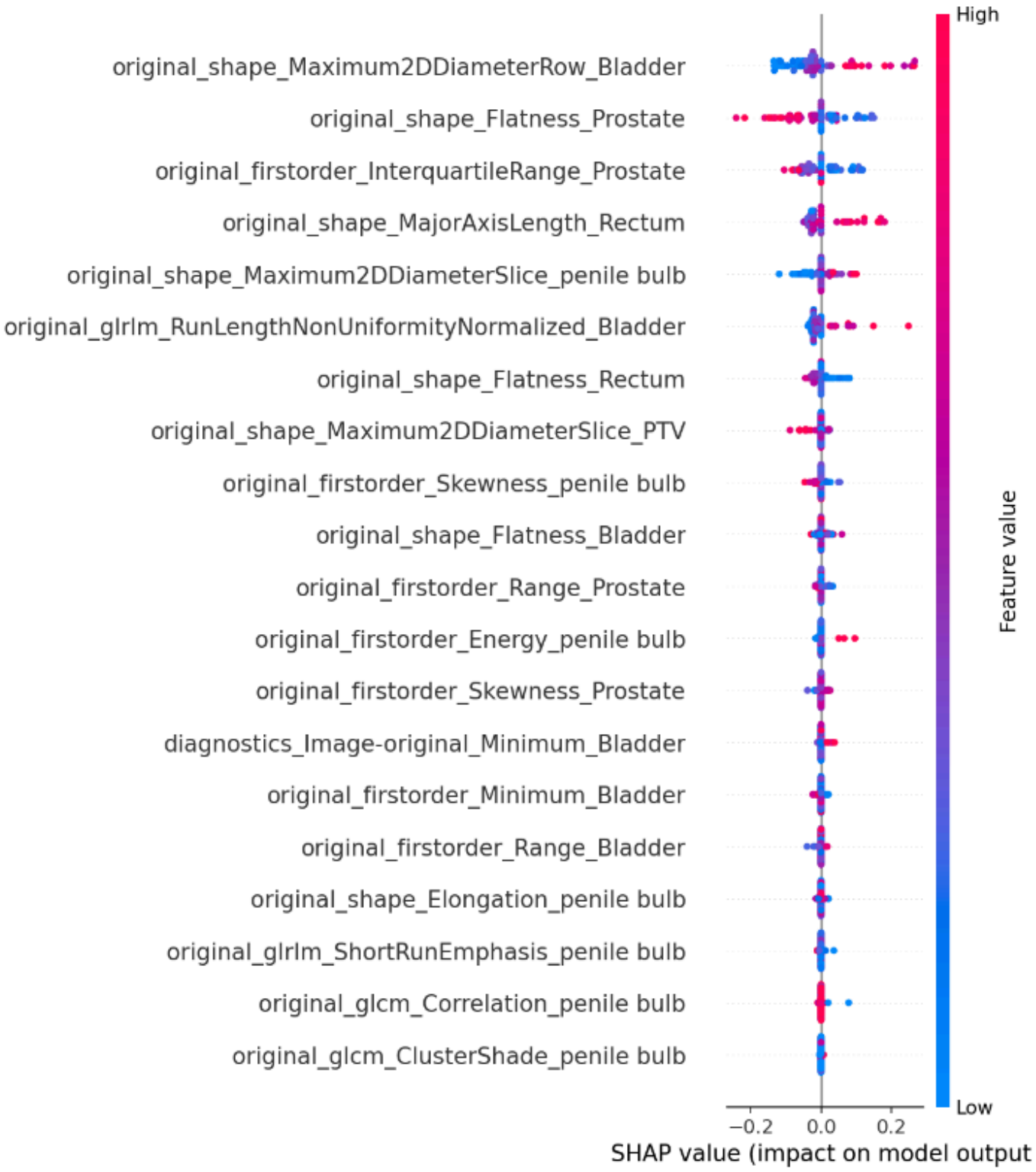


Figure 4

SHAP global summary (beeswarm) plot. Each dot represents one patient for one feature; the x-axis reports the SHAP value (feature contribution to the predicted probability of late GU toxicity, ϕ_{ij}), and color encodes the feature magnitude (low to high). Features are ordered by decreasing mean absolute SHAP value, highlighting the variables with the largest overall influence on the XGBoost model predictions. The apparent vertical dispersion of points within each feature row reflects multiple patients with similar

SHAP values and is introduced as vertical spread to avoid overplotting; only the horizontal axis has quantitative meaning. Features lower in the ranking show SHAP values concentrated near zero across most patients, consistent with their diminishing contribution to the model output.

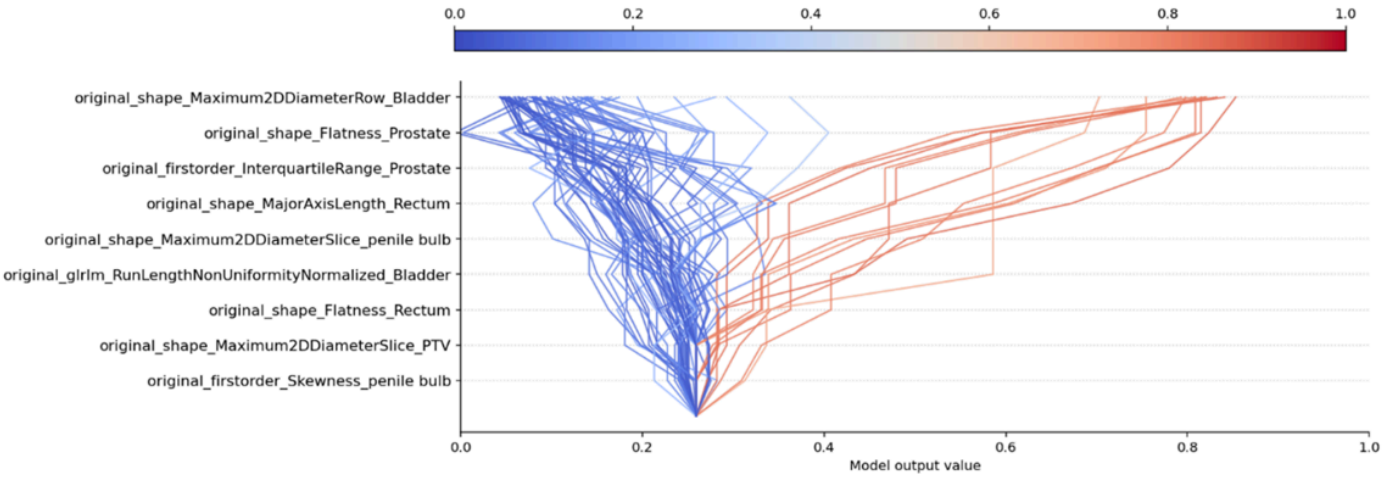


Figure 5. Global cumulative explanation of training-set predictions. Starting from the model expected value (baseline), SHAP values are added sequentially following the displayed feature order, producing one trajectory per patient ("spaghetti" lines). The x-axis shows the model output (predicted probability, $\hat{y}_i = \phi_0 + \sum_j \phi_{ij}$), and the y-axis lists features in the order they contribute to the cumulative prediction, illustrating how predictions diverge across patients.

Figure 5

See image above for figure legend

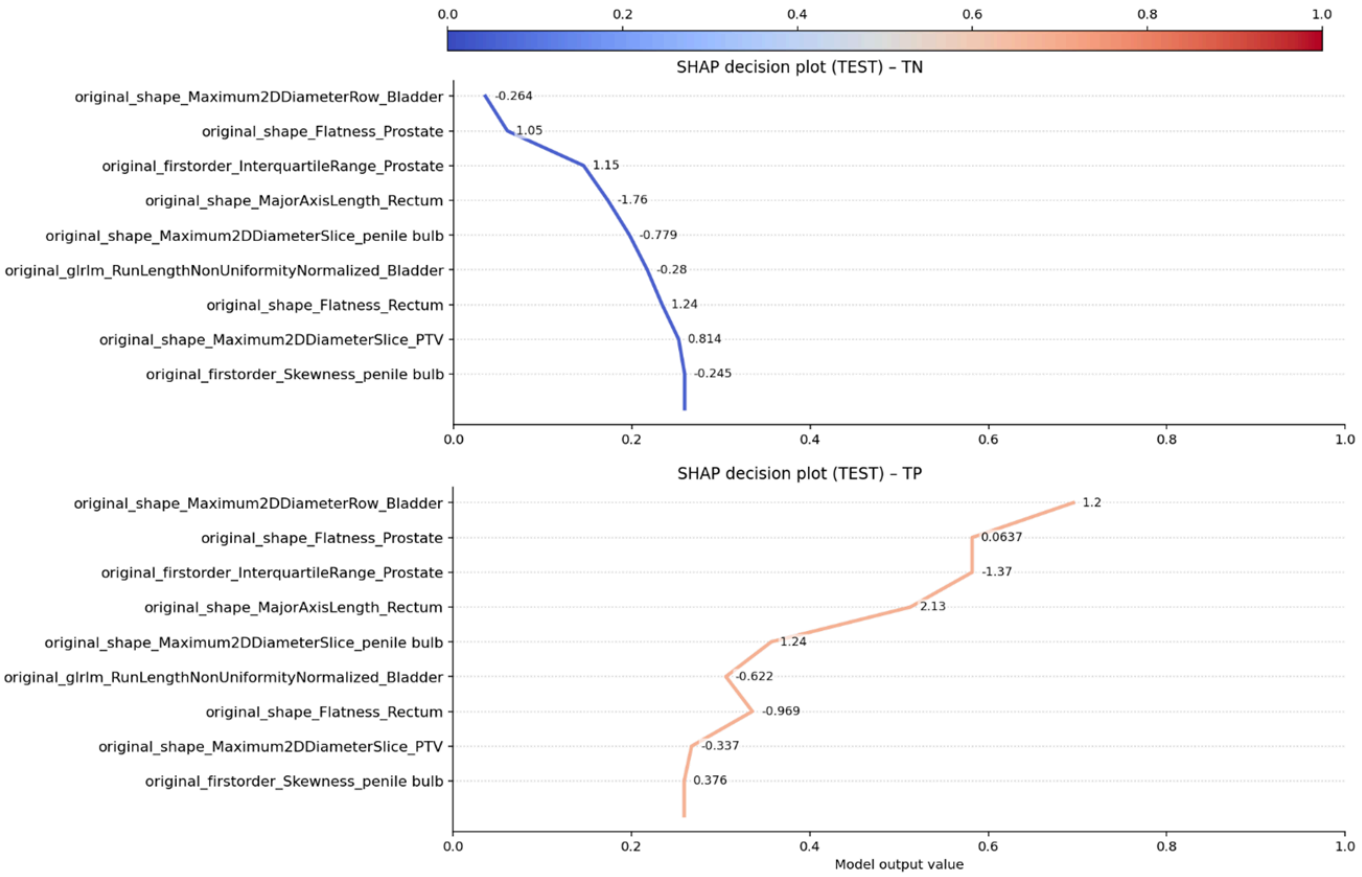


Figure 6

Patient-level SHAP decision plots for two representative test subjects (local explainability): a true negative (TN) and a true positive (TP). Each plot decomposes the individual prediction into a cumulative, stepwise path from the model expected value (baseline) to the final predicted probability by sequentially adding feature SHAP contributions in the displayed order. Patient-specific feature values are annotated at each step to provide traceability of the inputs driving the cumulative trajectories toward low (TN) and high (TP) model outputs.